K. Guesmi
D. Gozim
D. Mahi
A. Hamzaoui

J. Electrical Systems 6-2 (2010): x-xx

Regular paper

Nonlinear Phenomena Control in DC-DC Converters Using Dynamical Ramp

DC-DC power converters are characterized by cyclic switching of circuit configurations, which gives rise to a variety of nonlinear behaviors. Their occurrence in DC-DC power converters makes the system analysis, control and behavior prediction difficult. An enhanced modeling method allowing obtaining an accurate description of the converter behavior is presented in this paper. The principal of ramp compensation is introduced and dynamical compensation ramp is proposed to both suppress converter nonlinear phenomena and ensure the peak current regulation for a wide range of reference variation.

Keywords: boost converter, accurate model, compensation ramp, static slop, dynamical slop, nonlinear phenomena, bifurcation.

1. Introduction

DC-DC converters are electronic circuits allowing the electric energy conversion from one form to another by the commutation between a finite number of configurations. These systems can be considered as an indexed collection of continuous dynamical systems along with a mechanism for jumping or switching between them. Indeed, the system is characterized by continuous dynamics for each topology and discrete events corresponding to the switching conditions.

For the DC-DC converters there are two conduction modes; the discontinuous conduction mode (DCM) and the continuous one (CCM). In the DCM three topologies can be distinguished and two configurations in the CCM.

Generally, the DCM is used in the power factor correction (PFC) schemes due to the fact that can help to obtain a maximum of energy conversion. Whereas, in regulation schemes the CCM is preferred. Furthermore, the system analysis is easier in CCM than in DCM and the converter presents some features that do not appear in DCM as the right half plan zero in the output voltage to control transfer function [1].

DC-DC converters can be current-controlled (indirect control) or voltage-controlled (direct control). Based on linear control theory, classical controllers are predominantly used in industry due to their easy implementation, low cost and ability to achieve design objectives under some input specifications. However, the main drawback of such controllers is their inability to deal with nonlinear phenomena occurring under circuit parameters variation. Among many approaches used to handle this problem, Ott-Grebogi-Yorke method [2] stabilizes the chaotic system orbit through a small perturbation of a so-called control parameter. Pyragas method [3, 4] based on the use of delayed feedback control can also be used. Other approaches can be found in [5]. Most of these approaches stabilize the system orbit only for a given operating point and the control law depends on it. Thus, perturbations can drive the system away from the operating point and the controller falls to stabilize the system in its new orbit. Furthermore, they focus essentially on the system orbit stabilization and ignore other control performance aspects. To ensure the instability control and attain the desired reference, the use of compensation ramp is a standard practice [6-8]. Nevertheless, the control performance and the length of the stability range depend on the chosen slope of the ramp.

Corresponding author : K. Guesmi
CReSTIC, Université de Reims Champagne Ardenne, France.
guesmi@univ-reims.fr,

In this paper we use a boost converter as example and we choose the CCM as functioning mode. This converter will be controlled in current mode due to the fact that the converter is worthy in nonlinear phenomena in this mode. We propose in this paper a new and enhanced version of the compensation ramp technique to eliminate the drawbacks of the classical approach. An enhanced model of the converter is given in section II, whereas section III, is devoted to the presentation of the classical approach and the enhancements introduced to this last. In section IV, simulation results are presented to validate the proposed approach and to show its efficiency in term of current regulation, period-one region widening and nonlinear phenomena suppressing in the case of reference variation.

2. Converter Model

In this section, we present briefly an enhanced model used to describe the boost converter (Fig. 1) behavior accurately, with r_L, r_{SW}, r_{VD} and r_C denote the resistors of inductor L, switch sw, diode VD and capacitor C, respectively. R is the load, V_g the supply voltage, u_o the output voltage and i_L the input current.

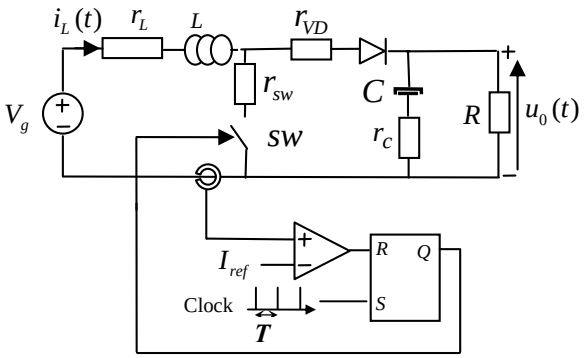

Fig. 1: Boost converter under current mode

In C.C.M. i.e., $i_L(t) > 0$, we have two configurations (Fig. 2) related to the switch sw position. In each one, the system can be described by a set of continuous differential equations. The transition from the first configuration to the second is conditioned by the reference reaching. A clock pulse is required to return to the first configuration (Fig. 1).

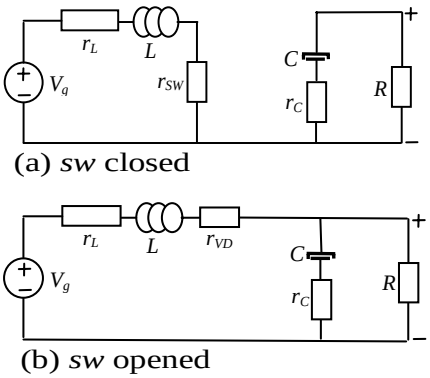

Fig. 2: Converter configurations in CCM

In the first configuration the switch *sw* is closed and the current i_L increases continuously until it reaches a reference current I_{ref}. At this point, the controller will open the switch *sw*, enabling the inductor discharging and the capacitor charging until the next clock pulse.

If we assume that, the dwell time in the first configuration is $t_1 = dT$, in the second configuration is $t_2 = d'T = (1-d)T$, the duty cycle is $d = t_1/T$ and *T* the clock cycle, the enhanced discrete model, proposed in [9], expresses the system state $x = [v_c \; i_L]^t$ (v_c: voltage across capacitor, i_L: inductor current) at the *(n+1)*th clock cycle by:

$$x((n+1)T) = \Phi_2(t_2)\Phi_1(t_1)x(nT) + \Phi_2(t_2)\int_{nT}^{(n+d)T}\Phi_1((n+d)T-\tau)B_1V_g\,d\tau + \int_{(n+d)T}^{(n+1)T}\Phi_2((n+1)T-\tau)B_2V_g\,d\tau \quad (1)$$

where

$$A_1 = \begin{bmatrix} -\frac{1}{C(R+rc)} & 0 \\ 0 & -\frac{r_L + r_{SW}}{L} \end{bmatrix},\; A_2 = \begin{bmatrix} -\frac{1}{C(R+r_C)} & \frac{R}{C(R+r_C)} \\ -\frac{R}{L(R+r_C)} & -\frac{r_L + r_{VD} + \frac{Rr_C}{R+r_C}}{L} \end{bmatrix},\; B_{1,2} = \begin{bmatrix} 0 & \frac{1}{L} \end{bmatrix}^t$$

are the state matrices and $\Phi_m(\alpha)_{m=1,2} = e^{A_m\alpha}$ the transition matrix in the configuration *m*. The exactitude of model (1) is mainly related to the computing method of the transition matrix $\Phi_m(t)$ and its integral term $\int_a^b \Phi_m\left(t_f - \tau\right)d\tau$. Based on Cayley-Hamilton theorem, exacts values of these two terms are given by the two flowcharts of figures 3 and 4

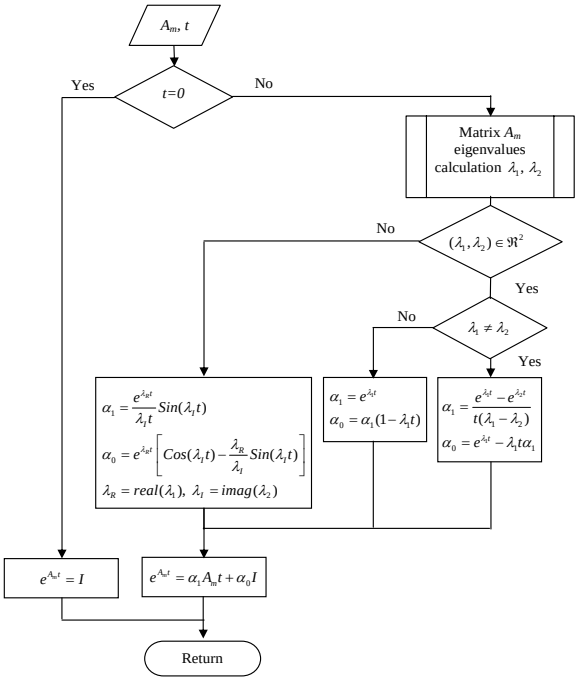

Fig. 3: Transition matrix flowchart

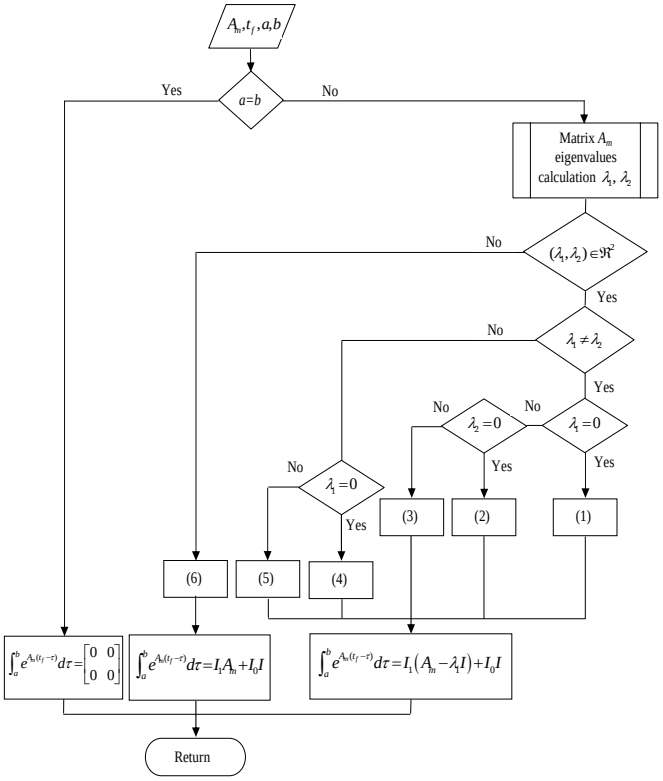

Fig. 4: Transition matrix integral flowchart

The expressions ((1)-(6)) in figure 4 are given by:

$$(1)\begin{cases} I_1 = -\dfrac{\left(\lambda_2(b-a) + e^{\lambda_2(t_f-b)} - e^{\lambda_2(t_f-a)}\right)}{\lambda_2^2} \\ I_0 = b - a \end{cases}, \quad (2)\begin{cases} I_1 = -\dfrac{\left(\lambda_1(b-a) + e^{\lambda_1(t_f-b)} - e^{\lambda_1(t_f-a)}\right)}{\lambda_1^2} \\ I_0 = -\dfrac{\left(e^{\lambda_1(t_f-b)} - e^{\lambda_1(t_f-a)}\right)}{\lambda_1} \end{cases},$$

$$(3)\begin{cases} I_1 = \dfrac{\lambda_2\left(e^{\lambda_1(t_f-b)} - e^{\lambda_1(t_f-a)}\right) + \lambda_1\left(e^{\lambda_2(t_f-a)} - e^{\lambda_2(t_f-b)}\right)}{\lambda_1\lambda_2\left(\lambda_2 - \lambda_1\right)} \\ I_0 = -\dfrac{\left(e^{\lambda_1(t_f-b)} - e^{\lambda_1(t_f-a)}\right)}{\lambda_1} \end{cases}, \quad (4)\begin{cases} I_1 = t_f(b-a) - \dfrac{b^2-a^2}{2} \\ I_0 = b - a \end{cases},$$

$$(5)\begin{cases} I_1 = \dfrac{\lambda_1\left(\left(b-t_f\right)e^{\lambda_1(t_f-b)} + \left(t_f-a\right)e^{\lambda_1(t_f-a)}\right) + e^{\lambda_1(t_f-b)} - e^{\lambda_1(t_f-a)}}{\lambda_1^2} \\ I_0 = -\left(\dfrac{e^{\lambda_1(t_f-b)} - e^{\lambda_1(t_f-a)}}{\lambda_1}\right) \end{cases},$$

$$(6)\begin{cases} I_1 = \dfrac{e^{\lambda_R(t_f-b)}\left[\lambda_I Cos\left(\lambda_I(t_f-b)\right)-\lambda_R Sin\left(\lambda_I(t_f-b)\right)\right]}{\lambda_I\left(\lambda_R^2+\lambda_I^2\right)} \\ \quad -\dfrac{e^{\lambda_R(t_f-a)}\left[\lambda_I Cos\left(\lambda_I(t_f-a)\right)-\lambda_R Sin\left(\lambda_I(t_f-a)\right)\right]}{\lambda_I\left(\lambda_R^2+\lambda_I^2\right)} \\ I_0 = \dfrac{\left(\lambda_R^2-\lambda_I^2\right)\left(e^{\lambda_R(t_f-b)}Sin\left(\lambda_I(t_f-b)\right)-e^{\lambda_R(t_f-a)}Sin\left(\lambda_I(t_f-a)\right)\right)}{\lambda_I\left(\lambda_R^2+\lambda_I^2\right)} \\ \quad -\dfrac{2\lambda_I\lambda_R\left(e^{\lambda_R(t_f-b)}Cos\left(\lambda_I(t_f-b)\right)-e^{\lambda_R(t_f-a)}Cos\left(\lambda_I(t_f-a)\right)\right)}{\lambda_I\left(\lambda_R^2+\lambda_I^2\right)} \end{cases}$$

where λ_R, λ_I designate respectively the real part and the imaginary one of the eigenvalue

In the next section, the classical method of ramp compensation is introduced at first; then the proposed enhancement to deal with nonlinear phenomena exhibited by the converter under current mode control is presented. The enhanced approach will be used with the presented model in order to ensure the current peak regulation and to eliminate the converter abnormal behaviors in a wide range of reference variation.

3. Enhancement of the Classical Approach

It's well known that the boost converter is unstable under current mode control for duty cycle values higher than 0.5 [1]. So, a standard practice to prevent this instability is the current programming or the use of the so-called compensation ramp [1, 6-8].
The circuit diagram of figure 5 gives the principal of this concept. In addition to the boost converter, the circuit contains:

- an outer loop (voltage loop) allowing obtaining a reference signal (voltage) corresponding to the reference current.
- a compensation bloc to modify the value obtained from the voltage loop in order to prevent the instability by adding a compensation ramp with slop S_c to the reference signal.
- an inner loop that close and open the switch *sw* by comparing the inductance current to the compensation bloc output signal.

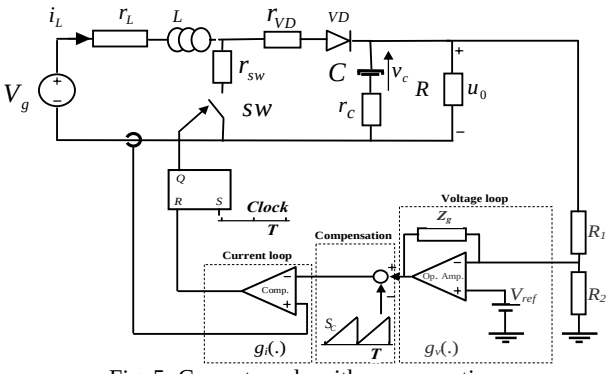

Fig. 5: Current mode with compensation

The use of compensation ramp leads in steady state to the system typical response (i_L) given by figure 6. To asses about stability, the duty cycle is chosen higher than 0.5

($D > 0.5$), the solid line refers to the case of unperturbed system whereas; the dashed line represents the case of perturbed system.

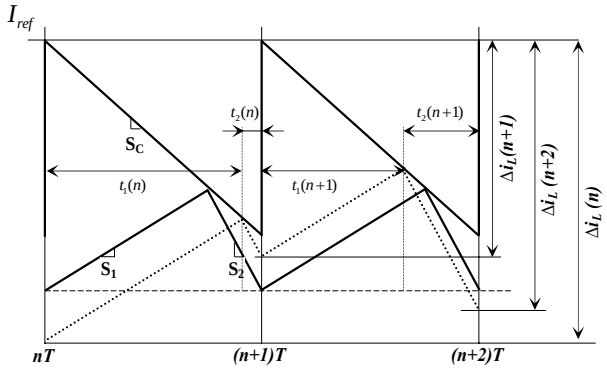

Fig. 6: Typical response using compensation ramp

By examination of the waveform related to the perturbed system we can remark (Fig. 6) that the compensation ramp damps the perturbation propagation. This indicates that the inductor current deviation at each clock period from the reference I_{ref} is given as:

$$\Delta i_L(n) = (S_1 + S_C)t_1(n) \tag{2}$$

$$\Delta i_L(n+1) = S_2 t_2(n) + S_C t_1(n) \tag{3}$$

where $t_1(n)$, $t_2(n)$ are the dwell times in the first and second configuration respectively during the n^{th} clock period and they are given by: $t_1(n) = D(n)T$ and $t_2(n) = (1 - D(n))T$.

We can combine (2) and (3) to obtain the following recurrent description of the system:

$$\Delta i_L(n+1) = \frac{S_C - S_2}{S_C + S_1}\Delta i_L(n) + S_2 T \tag{4}$$

Hence, in order to damp the perturbation, the choice of the slop of the compensation ramp must verify:

$$\frac{S_2 - S_C}{S_1 + S_C} < 1 \tag{5}$$

From this inequality we can obtain the stability condition in absence of ramp compensation ($S_C = 0$) which is: $D < 0.5$. In the opposite case ($S_C \neq 0$) the ramp slop must satisfy (5) which mean:

$$S_C > S_1\left(\frac{1}{2(1-D)} - 1\right) \text{ or } S_C > S_2\left(1 - \frac{1}{2D}\right) \tag{6}$$

Generally, the outer-loop output signal (Fig. 5) is considered as constant compared to the fast dynamics of the inner-loop. So, we can consider the inner-loop only to asses about the converter fast scale instabilities. Furthermore, if the converter operates away from the point $D \approx 1$, where the imperfection effect is important, the internal resistors of elements (r_L, r_C, r_{VD}, r_{SW}) can be neglected and the control law is given by:

$$d(n) = \frac{I_{ref} - i_L(n)}{T(S_1 + S_C)} \tag{7}$$

Using the control law (7) with the choice of S_C according to (6) allows damping the perturbation propagation and obtaining a stable behavior of the converter as shown in figure 6. However, this technique has some drawbacks. Indeed, expression (6) gives a semi-open interval for the slop; choice may be by a trial and error procedure or by the use of an

optimization algorithm to obtain an optimal value for the slop. Moreover, the static slop needs to be updated or changed every time there was deviation from or variation of the operating point to keep the desired performance. For these reasons, we propose the use of dynamical slop. A candidate law to update the slop is simple law of the form PI. Hence, the slop can be defined by:

$$S_C = \alpha S_1 \tag{8}$$

with α a factor calculated by the PI law for the n^{th} clock cycle as follows:

$$\alpha(n) = K_p e(n) + K_I \sum_{i=0}^{n-1} e(i) \tag{9}$$

where $e(n) = i_L(n) - i_L(n-1)$, K_p and K_I are respectively the proportional and integral gains that can obtained by classical approaches like Zigler-Nichols method.

In the next section we evaluate the proposed approach efficiency and we asses about the obtained performances.

4. Simulation Results

To illustrate the improvement of the system behavior using the proposed dynamical ramp, let us consider the Boost converter with: $V_g = 5\,\mathrm{V}$, $L = 1.5\,mH$, $R = 40\Omega$, $C = 20\mu F$ and the switching frequency $f_{sw} = 1/T = 10KHz$.

Imperfection of the converter elements is neglected ($r_L = r_C = r_{VD} = r_{SW} = 0$). The converter elements values are chosen to satisfy the condition: $2L/RT > 4/27$ that ensures the converter functioning in CCM.

Using the model developed in paragraph 2, the converter original behavior can be explored under the classical feedback of figure 1 ($S_C = 0$) to reach a reference current I_{ref}. The obtained bifurcation diagram is given in figure 7.

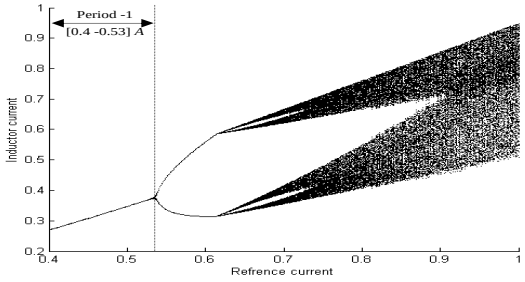

Fig. 7: Original behavior of the converter 1T-2T-Chaos via quasi 4T

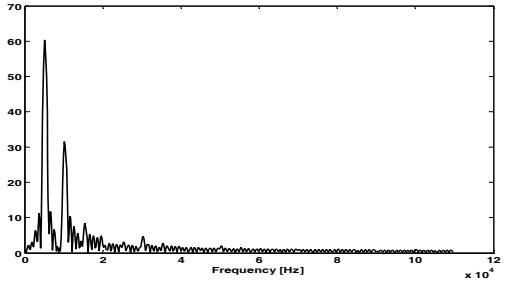

Fig. 8: Fourier spectrum for I_{ref}=0.68A

The obtained results (Fig. 7) shows that the converter exhibit period 1 behavior (1T) followed by period 2 and chaos via quasi-period 4. We note that the observed quasi periodicity is identified by means of Fourier spectrum analysis. Indeed, for a reference current equal to 0.68A, the Fourier spectrum is shown in figure 8, where we can note that the frequency ratio is irrational and equal to 1.9413, confirming the existence of quasi periodicity oscillations in the system response.

Now we present a comparison study between the static ramp and dynamical ramp in terms of system performance. Table 1 summarizes the obtained results in this comparative study. From this table, we can remark clearly that the dynamical ramp enhances the system dynamics and allows obtaining a current error 7 times less than the one ensured by the static ramp.

Tab. 1: Performance under static and dynamical ramps

	Static ramp $S_C = 0.54\,S_1$	Dynamical ramp
Current error: I_{ref} - $Peak(i_L)$	84.1 [mA]	11.5 [mA]
Average output voltage: $< v_C >_T$	9.367 [V]	10.053 [V]
Response time	0.6 [ms]	0.6 [ms]

We note that the system performance with static ramp can be enhanced by reducing the ramp slop; however, we enhance the performance by hand and we squeeze the length of period 1 zone by the other hand.

After many simulations we remarked that the slop $S_C = 0.54\,S_1$ represent a trade-off between the system performance and the length of period 1 zone. Using this slop, figure 9 illustrates the obtained bifurcation diagram.

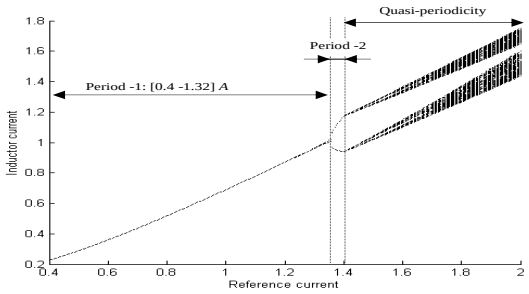

Fig. 9: Bifurcation diagram using static ramp

From this figure we remark the enhancement achieved by the static slop to damp perturbation and to shift the first bifurcation. Indeed, the period one in the original behavior is ensured for reference values from 0.4*A* to 0.53*A* (Fig. 7), whereas the use of static ramp allows obtaining a wider period one zone from 0.4*A* to 1.32*A* (Fig. 9). Moreover, this technique suppresses the chaotic behavior from the area of interest and we have only a quasi periodicity oscillation as confirmed by the Lyapunov exponent depicted in figure 10.

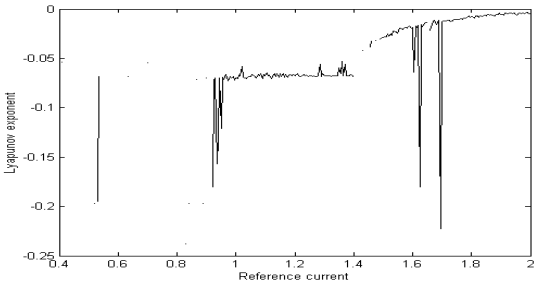

Fig. 10: Lyapunov exponent for static ramp

Now if we use, instead, the dynamical slop, that vary according to the system dynamics, we obtain the bifurcation diagram of figure 11.

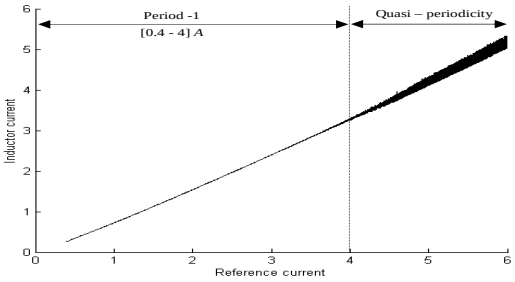

Fig. 11: Bifurcation diagram using dynamical ramp

Compared to results of figures 7 and 9, the converter behavior under the dynamical ramp (Fig. 11) has been enhanced and the system structural stability is ensured. Indeed, we note the total undesirable phenomena elimination and the period one (1T) region widening from $[0.4, 0.53]A$ in the original behavior and $[0.4, 1.32]A$ under static ramp to $[0.4, 4.1]A$ under the dynamical ramp (Fig. 11). This facilitates the converter behavior prediction and analysis. The abnormal behaviors are efficiently eliminated from the area of interest and we have only quasi periodic oscillations and there is no chaotic behavior as shown by Lyapunov exponent given in figure 12. Moreover, by comparing results of figure 11 to those of figure 9 we remark that with the dynamical slop we have lower amplitude of the quasi periodic oscillations than the one ensured by the static ramp.

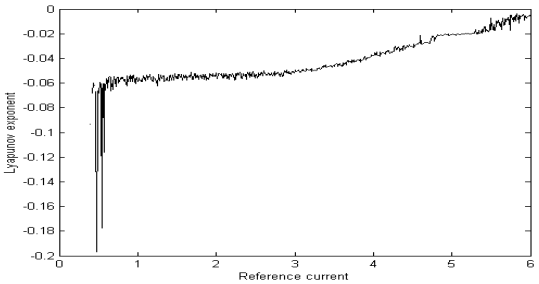

Fig. 12: Lyapunov exponent using dynamical ramp

Other simulation results, not depicted in this work, shows that obtained structural stability is also ensured by the proposed dynamical slop in the case of varying the other parameters of the converter such as supply voltage, inductor and load.

5. Conclusion

In this paper, a dynamical ramp controller for a boost converter, allowing the nonlinear phenomena suppression in the operating domain, was proposed. An adequate model was used to obtain a more accurate exploration of the different undesirable nonlinear phenomena. The principal of ramp compensation was explained. Enhancement is given by varying the slop of the ramp according to the system dynamics. A PI law is adopted for the slop variation. The PI gains are chosen to ensure the converter peak current to be closer to the reference in wide range of operating point variation. Compared to the original behavior of the system and to the one ensured by static ramp, simulation results showed the dynamical ramp ability to efficiently suppress the undesirable nonlinear phenomena in the operating domain, to ensure the desired regulation performance and to enlarge the desired period one operating domain. Thus, the system behavior prediction and analysis become easier.

References

[1] R. W. Erickson and D. Maksimovic, "Fundamentals of Power Electronics," Kluwer Academic Publishers, Boston, Dordrecht, London, 1999.

[2] E. Ott, C. Grebogi, J. A.Yorke, "Controlling chaos, " *Physical Review Letters*, pp. 1196-1199, 1990.

[3] K. Pyragas, "Continuous control of chaos by self-controlling feedback, " *Physical Letters A*, pp. 421-428, 1992

[4] K. Pyragas, "Control of chaos via an unstable delayed feedback controller," *Physics Review Letters*, pp. 2265-2268, 2001

[5] A. L. Fradkov, R. J.Evans, "Control of chaos: methods and applications in engineering, " *Annual Review in Control*, pp. 33-56, 2005.

[6] C. K. Tse, "Flip Bifurcation and Chaos in three-state boost switching regulators, " *IEEE Trans. On Circuits and Systems*, pp. 16-23, 1994.

[7] I. Zafrany and S. Ben-Yaakov, "A chaos model of subharmonic oscillations in current mode pwm boost converters", IEEE Power Electronics Specialists Conference, pp. 1111-1117, Atlanta, 1995.

[8] Banerjee S, Verghese GC. "Nonlinear phenomena in power electronics," IEEE press: NJ (USA), 2001.

[9] K. Guesmi, N. Essounbouli, N. Manamanni, A. Hamzaoui and J. Zaytoon, "An enhanced modelling approach for DC-DC converters", Proceedings Of IFAC conference on analysis and control of chaotic systems, Reims (France), 2006.